Membrane Characterization via Evapoporometry (EP) and Liquid-Liquid Displacement Porosimetry (LLDP) Techniques

Melike Begum Tanis-Kanbur[a,b,c], René I. Peinador[d], Xiao Hu[e,f], José I. Calvo[g] , Jia Wei Chew[a,c,*]

[a] *Singapore Membrane Technology Centre, Nanyang Environment and Water Research Institute, Nanyang Technological University, 637141, Singapore*

[b] *Interdisciplinary Graduate School, Nanyang Technological University, 639798, Singapore*

[c] *School of Chemical and Biomedical Engineering, Nanyang Technological University, 637459, Singapore*

[d] *Institut de la Filtration et des Techniques Séparatives (IFTS), Rue Marcel Pagnol, 47510, Foulayronnes, France*

[e] *Environmental Chemistry and Materials Centre, Nanyang Environment and Water Research Institute, Nanyang Technological University, Singapore 637141, Singapore*

[f] *School of Materials Science and Engineering, Nanyang Technological University, Singapore 639798, Singapore*

[g] *Departamento de Física Aplicada, ETSIIAA, Universidad de Valladolid, 34071 Palencia, Spain*

** Corresponding author: JChew@ntu.edu.sg; +65 6316 8916; School of Chemical and Biomedical Engineering, Nanyang Technological University, 637459, Singapore*

Abstract

To comparatively assess the Evapoporometry (EP) technique vis-à-vis the Liquid-Liquid Displacement Porosimety (LLDP) technique, the pore size distributions, mean pore diameters (d_{avg}) and porosities of five polymeric (namely, nylon, PES, PTFE, PET and PVDF) and one inorganic (namely, alumina) UF/tight MF membranes were quantified by both techniques. For all the membranes, the pore size ranges were generally narrower and the pore size distributions had distinctive peaks for the LLDP technique. For the nylon, PES and PTFE membranes, the d_{avg} values obtained from the two techniques agreed well. However, for the PET and PVDF membranes, the differences were twofold due to the higher pressure needed for the LLDP tests. Specifically, for PET, the d_{avg} value obtained via EP was half that via LLDP, because the higher pressure compacted the lower mechanical strength polymer, leading to pore closure. On the other hand, for PVDF, due to the rubber nature, the higher pressure caused the pores to be stretched, leading to larger pores. As for the alumina membrane, because of the more ideal cylindrical pores, the d^4-weighting of the LLDP measurement gave a greater d_{avg} value than

that of the d^2-weighting of the EP measurement. Also, porosity measurements were erroneous for LLDP if the active layer cannot be precisely quantified. With respect to MWCO, while EP does not explicitly quantify this, the LLDP generally over-estimated the values, because of the errors associated with the measurement of the first (largest) pores at the lowest pressures.

Keywords: Pore size distribution (PSD); wettability; surface tension; membrane characterization; porosity

1. Introduction

Membrane technology has been gaining importance as a promising alternative to the conventional separation methods, because of well-recognized advantages such as lesser complexity, lower operation costs, fewer effluents (thus a more environment-friendly process), ease of control and lower energy demand [1]. In most membrane processes, pore sizes play a key role in controlling the separation process with respect to the most important performance parameters of permeability and selectivity. In terms of pore sizes, membrane-filtration can be classified into microfiltration (MF; 0.1 to 5 μm), ultrafiltration (UF; 1 to 100 nm), nanofiltration (NF; 0.5 to 10 nm), and reverse osmosis (RO; non-porous) [2]. Unsurprisingly many methods are available for the measurement of pore sizes, as overviewed in Fig. 1. The direct methods include the microscopic techniques (e.g., SEM, TEM, AFM, STM) [3-5] and spectroscopic techniques (e.g., EIS, PAS, RS, NMR) [6-19]. On the other hand, indirect methods are also available, which are based on some theoretical basis to convert measured parameters into pore sizes. The focus of this study is on the use of indirect methods to characterize UF/tight MF membranes.

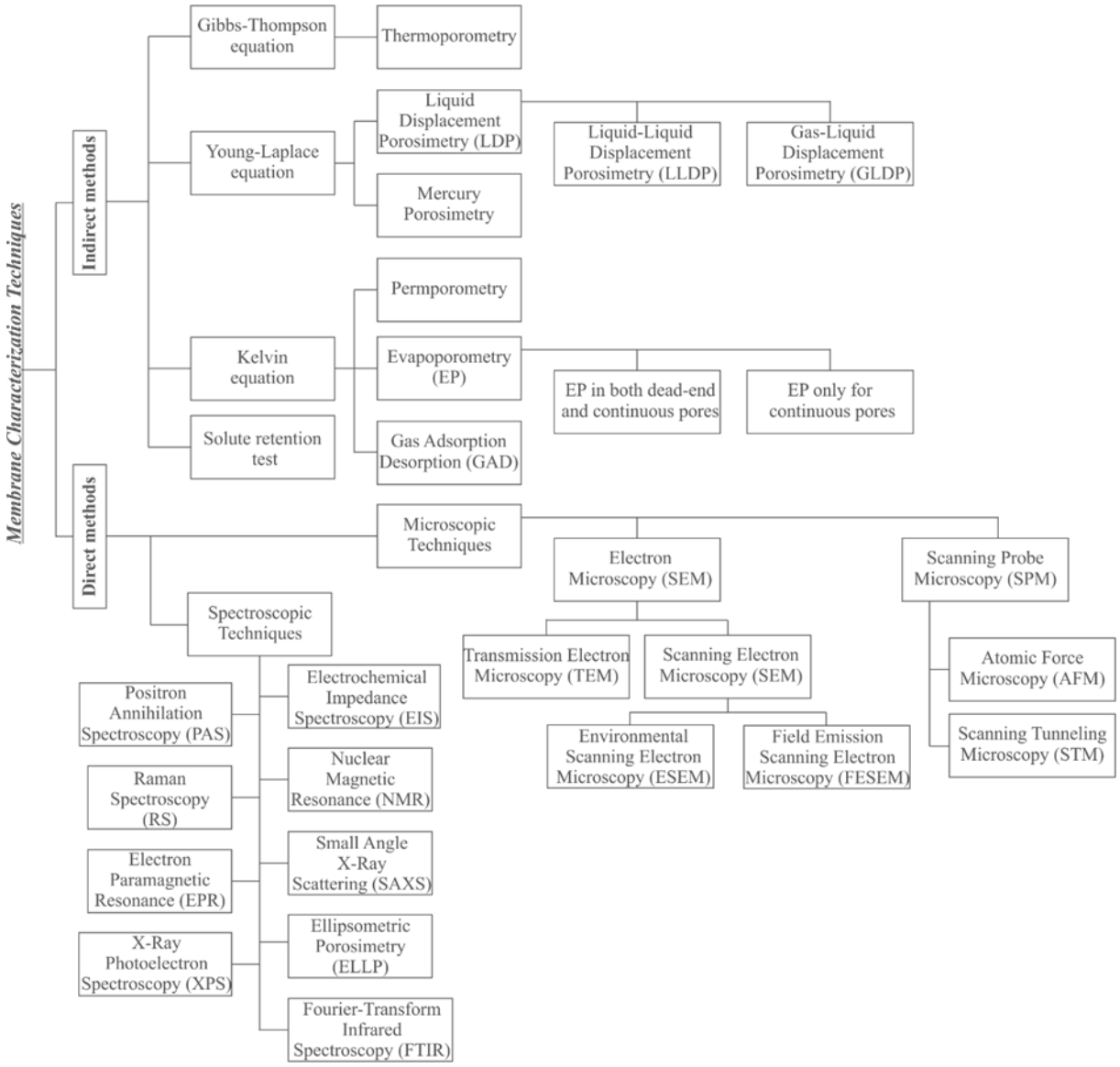

Figure 1: Pore size distribution (PSD) measurement techniques for membranes.

Some examples of the indirect methods based on the Kelvin equation are the Gas Adsorption-Desorption (GAD), permporometry, and evapoporometry (EP) techniques. In the GAD method, the membrane pores are filled via capillary condensation and adsorption due to the pressure increment [20, 21]. The Kelvin equation determines the evaporation of liquid from the largest pores to the smallest pores when decreasing the pressure, and the desorbed gas amount is used to calculate the volume of pores for a given diameter. Requirements for both volume and pressure measurements (for the gas) limit the accuracy of this method [22]. The

permporometry technique includes a condensable gas like the GAD method, but a non-condensable gas is also applied in order to measure only the continuous pores and exclude the dead-end pores [22-25]. The flow of non-condensable gas makes it possible to observe the continuous pores that cannot be observed via the GAD method. Another relatively new Kelvin equation-based technique is the EP method that requires a volatile wetting liquid for characterizing both inorganic and polymeric membranes [26-32]. In the EP method, progressive evaporation is observed from the largest to smallest pores by means of a microbalance; then, the mass associated with each pore size can be obtained using the Kelvin equation. The measurement of mass provides for high accuracy. PSDs can be obtained from multi-bore and hollow fiber membranes [31], fouled membranes [26], backwashed membranes [28], and biofouling layers [29]. Recently, EP has been advanced to distinguish continuous from dead-ended pores [33].

Gas-liquid displacement porosimetry (GLDP), liquid-liquid displacement porosimetry (LLDP), and mercury porosimetry are examples of other indirect methods based on the Young-Laplace equation. Mercury is used as a non-wetting fluid for the well-known mercury porosimetry method [34-37], with the progressive pore filling from the largest pores to the smallest pores. In order to provide the entrance of mercury into the pores, especially the smallest ones, high pressures are required; hence, the PSD of compressible polymeric membranes can be altered during the mercury porosimetry tests. Moreover, since mercury is toxic, samples so analyzed must be properly discarded. On the other hand, liquid displacement porosimetry (LDP) uses a non-toxic wetting fluid to completely wet the membrane, which is later emptied by dispelling the wetting liquid with an immiscible one. Two different methods arise from this concept, namely, the Gas Liquid Displacement Porosimetry (GLDP) or Liquid-liquid Displacement Porosimetry (LLDP), depending on whether the displacing fluid is a liquid or a gas. In both methods, by increasing the pressure applied by the displacing fluid, the wetting

fluid saturating the membrane pores is progressively displaced from the largest pores to the smallest pores; thereby, the fluid flow through the pores are measured. The Young-Laplace equation is used to correlate the diameter of the pores just emptied with the pressure applied. Both LDP techniques can be applied for MF membranes well. Unfortunately, for tight UF membranes, the GLDP method cannot be used for tight UF membranes, since the high pressures necessary to empty the small nanometer-sized pores (due to the relatively high surface tension of the air-liquid interface) may alter the PSDs of UF membranes [38-40]. Fortunately, LLDP is able to by requiring a significantly reduced pressure to displace the liquid, because of the dramatically different surface tension at the liquid-liquid interface relative to that at the gas-liquid interface [3, 41-50].

Since Kelvin equation - based EP and Young-Laplace equation - based LLDP are two promising PSD characterization techniques with recent advances, it is timely to comparatively assess the obtained results. Accordingly, this study was targeted at evaluating six membranes, of which five are polymeric and one inorganic, using both techniques. Pore size distributions, mean pore diameters and porosities from both techniques are juxtaposed, and the underlying differences explained. The molecular weight cut-off (MWCO) was also quantified by LLDP and compared to reported values.

2. Theory

2.1. Evapoporometry (EP) principles

The evaporation of a volatile wetting liquid from a saturated membrane naturally occurs progressively from the largest pores to the smallest pores. The EP method measures the mass loss rate due to evaporation of the volatile wetting liquid from the pores, from which the pore size distribution (PSD) can determined by the Kelvin equation [51-53]:

$$\ln \frac{P_A}{P_A^0} = -\frac{4V\gamma \cos\theta}{dRT} \quad (1)$$

where P_A is the vapor pressure of the volatile wetting liquid, P_A^0 is the normal vapor pressure of the volatile wetting liquid, V is the molar volume of liquid, and T is the absolute temperature. According to Eq. (1), the vapor pressure of the liquid decreases with pore diameter (d) and d can be calculated if P_A is known. Eq. (1) can be re-cast in terms of evaporation rate (W_A) instead of vapor pressure as follows:

$$d = -\frac{4V\gamma\cos\theta}{RT\ln\frac{W_A}{W_A^0}} \quad (2)$$

Therefore, the PSD can be quantified by measuring the evaporation rate, W_A, from the saturated membrane using a high-resolution balance [27].

2.2. Liquid-liquid displacement porosimetry (LLDP) principles

The LLDP technique is based on the well-known Young-Laplace equation which governs the pressure difference at the interface between two immiscible fluids. For a general geometry, the pressure difference at the interface (ΔP) can be expressed as:

$$\Delta P = 2\gamma \mathrm{H} \quad (3)$$

where γ is the interfacial surface tension of both immiscible fluids; and H is the interface curvature, which from geometric considerations, can be expressed as:

$$H = \frac{1}{2}\left(\frac{1}{r_1} + \frac{1}{r_2}\right) \quad (4)$$

where r_1 and r_2 are the principal radii of curvatures for the surface. For the case of a cylindrical tube (i.e., the ideal pore), the Young-Laplace equation must be modified to include the contact angle (θ) between the spherical meniscus formed in the inner pore and the pore wall, resulting in:

$$\Delta P = \frac{4\gamma\cos\theta}{d} \quad (5)$$

For the case of a membrane, made up of a bunch of pores that could be simplified as straight-through cylinders with a range of diameters, Eq. (5) can be applied to determine the PSD through measuring the ΔP values.

Correspondingly, the LLDP technique requires a wetting liquid that is immiscible with another liquid that displaces it from the pores. When the pressure of the displacing liquid applied to the membrane is gradually increased, the wetting liquid will be displaced from the largest pores first, then progressively to the smallest ones. Applying Eq. (5) to each pressure step allows for the size of the pores to be determined. Consequently, a good selection of the pair of liquids to be used for wetting and displacing is key to the successful implementation of this characterization method. Liquids pairs with very low interfacial tension [48] are more suitable for testing membranes with pore sizes in the nanometer range. For example, according to Young-Laplace equation, for the Water/Isobutanol liquid pair (γ=1.7 mN/m), and assuming complete membrane wetting (i.e., $\theta = 0$), pores with diameters of 50 nm (i.e., in the ultrafiltration (UF) range) will be expelled out by the displacing liquid at a pressure of ~1.3 bar, which is reasonably low, particularly for membranes operating at higher pressures.

3. Materials and Methods

3.1.Membranes

Six flat-sheet membranes were characterized. They were selected such that the pore sizes span most of the UF range, and also made of different materials, namely, Nylon, PTFE, PVDF, PES, PET, and Al_2O_3 (commercialized by Whatman as Anopore®). The information available on the membranes are given in Table 1. In the case of the Nylon, PTFE and PET membranes, these were pre-commercialized and under-going research under a non-disclosure agreement

that prevents the publishing of the company name (designated as 'Company A' in Table 1). All membranes were received in the form of flat sheets, except the Al_2O_3 ones that were available as circularly shaped samples, which were cut to the required diameter to be used in both porosimetric devices, namely, EP and LLDP. For each membrane and technique, at least three fresh samples from the same batch, were analyzed and results were averaged. From the standard deviation of results, percentage of error were calculated as: Standard deviation / Average value.

Table 1. Characteristics of the six membranes analyzed.

Material	Manufacturer	Pore Range	Nominal MWCO/Pore size	Type
Nylon	Company A	UF	Not available	Flat Sheet
PES	Pall Corporation	UF	300 kDa	Flat Sheet
PTFE	Company A	UF	Not available	Flat Sheet
PET	Company A	UF	Not available	Flat Sheet
PVDF	Synder Filtration	UF	100 kDa	Flat Sheet
Al_2O_3	Whatman	MF	0.1 µm	Disk

3.2. Evapoporometry (EP) method

The EP setup (Fig. 2a) was the same as that reported in previous studies [26-28, 30-33]. In order to maintain equilibrium saturation at the interface between the gas and liquid phases in the pores that evaporation is occurring from, the membrane was housed in a test cell (Fig. 2b), which had a lid with a small hole of 6 mm to limit the mass-transfer rate from the test cell [27]. Specifically, the test cell had an inner diameter of 35 mm and height of 25 mm, and was made of polytetrafluoroethylene (PTFE) to avoid wetting by the volatile liquid. A microbalance with a resolution of 10 µg (Mettler-Toledo; XP56) was used to measure the progressive loss of mass due to evaporation. Other components of the setup (Fig. 2a) included an incubator (Yihder; LE-150D) to keep the temperature constant (29 °C) during each run, and an anti-vibration table to avoid disturbances to the microbalance. The measurement of the mass values from the microbalance was constantly recorded every 10 s via the Balance Link Software (Mettler Toledo). Granular activated carbon (GAC; Sigma-Aldrich) was placed on a stand above the test

182 cell in the microbalance chamber (Fig. 2b) to reduce the vapor concentration of the volatile
183 wetting liquids in the chamber. The volatile wetting liquid used was isopropyl alcohol (IPA;
184 99.9%; Sigma-Aldrich), which was also used in several prior EP studies [26-28, 32].

185 The membranes were cut into circles each with a diameter of 40 mm, then positioned
186 between the flanges at the bottom of the test cell, after which a thin film of vacuum grease (Dow
187 Corning) was applied before clamping the flanges to prevent evaporation of the volatile wetting
188 liquid from the periphery. Subsequently, the volatile wetting liquid was added to the top of the
189 clamped membrane to ensure the entire membrane was immersed in a free-standing liquid layer
190 (i.e., excess liquid after pore-wetting), whose evaporation rate was used to determine the mass-
191 transfer coefficient of the diffusion test cell (Fig. 4b). The data-analysis protocol was similar to
192 earlier studies [26-28, 30-32]. In brief, the steps were: (i) plot W_A, determined from the slope of
193 the mass loss versus time plot, versus time; (ii) determine the evaporation rate for the free-
194 standing liquid layer (W_{A0}) from the portion of the mass versus time plot over which W_A is
195 constant; (iii) determine the onset of pore-draining (i.e., from the largest pores) by the point at
196 which the instantaneous mass of the liquid is equal to that in the saturated membranes; (iv)
197 determine the instantaneous values of W_A and the corresponding pore diameter (d) using Eq.
198 (2); and (v) collate the measured pore diameters (d) into 5 nm bins, and plot the cumulative
199 mass in each pore size bin as a function of the pore diameter (d) to determine the PSD.

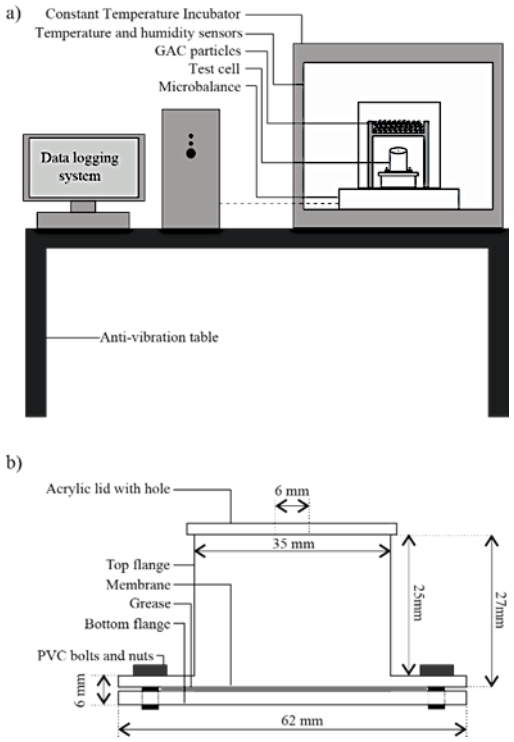

200

201 Figure 2. Schematic of the (a) EP experimental setup; and (b) EP test cell.

202

203 **3.3.Liquid-liquid displacement porosimetry (LLDP) method**

204 The Fluid-Fluid Porometer (FFP; model PRM-8710®) used in the LLDP analysis
205 consisted of an automated pressure constant device suitable for Gas/Liquid and Liquid/Liquid
206 tests (Fig. 3). It has been developed and commercialized by IFTS®, and it is right now the only
207 device available in the market [54]. The device is configured for testing of pore sizes down to
208 4 nm and uses relatively low pressures for the characterization of porous membranes in the UF
209 range. The equipment allows for implementing very stable pressure and leads to very accurate
210 measurement of resulting fluxes by using an analytical balance (Sartorius® Practum, accuracy
211 of 1 mg). It is able to determine several important parameters related with PSD, including mean
212 pore diameter, peak pore size, pore size distribution, solvent permeability, and droplet point. It
213 also can be adapted to analyze various membrane types, including hollow fiber, tubular and flat
214 sheet.

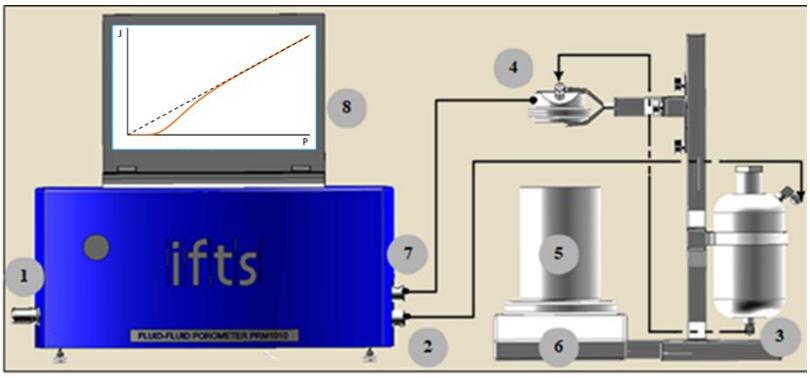

Figure 3. Schematic of the IFTS FFP®: (1) air supply; (2) air pressure tank; (3) feed line; (4) membrane-housing cell; (5) disposal; (6) analytical balance; (7) retention line (pressure sensor); and (8) IFTS LLDP software

In this study, flat sheet membranes were characterized by a membrane filtration cell with a diameter of 47 mm. LLDP experiments were performed according usual procedure, [44-46]. In these experiments, the applied pressure is increased gradually, and the membrane permeability, defined as the flux to pressure ratio, monitored. The differential increase of permeability is defined as:

$$\Delta L_k = \frac{L_k - L_{k-1}}{L_{tot}} \quad (6)$$

where L_k is the permeability of the k^{th} step ($k = 1, 2, \ldots, i$) and L_{tot} is the final permeability (asymptotic permeability) in the final step (i.e., $k = i$). The value of the asymptotic permeability, L_{tot}, corresponds to the moment when the wetting liquid is drained away from all the membrane pores. It must be noted that the calculation of ΔL_k only accounted for positive values, as negative ones mean that yet opened pores were again closing or non-contributing to total permeability. The plot of contributions to total permeability for each pore size opened (then for each pressure increase step) can be understood as a pore size distribution in terms of flow (or permeability). From such a permeability distribution, PSDs in terms of pore number can be obtained by application of the calculation algorithm developed by Grabar and Nikitine [55] to determine the

number of pores open to flow in each increment n_k. The algorithm makes use of the Hagen-Poiseuille model for convective flow through pores, which needs to assume cylindrical geometry for the pores and a continuous curve of permeability variation for derivation. In practical tests, experiments lead to a bunch of discrete data pairs (i.e., flux versus pressure), so the conversion algorithm must be converted from a continuous variation to incremental variations. This leads to the following equation:

$$n_k(d) = \frac{256\eta l}{\pi d_k^5}\Delta L_k \quad (7)$$

where η is dynamic viscosity of the displacing liquid; l is the length of the pore; and d_k is the pore diameter of the pores opened up to the k^{th} step. It should be noted that the l value equals to the active layer thickness and membrane thickness for the asymmetric and symmetric membrane types, respectively. For each increasing pressure step, ΔP_k, a corresponding volumetric flow was measured, Q_k, and pore diameter (d_k) values were obtained.

A very stable 1:1 (v/v) binary mixture composed by water/isobutanol (γ =1.7 mN/m) was used. All liquids were of reagent grade and used as received without further purification (Sigma- Aldrich®: Purity ≥ 98.5 %). The temperature was kept constant at 22 °C (± 0.1 °C). The mixtures were prepared by adding targeted amounts of Milli-Q®grade water and alcohol into a separatory funnel, and shaking it vigorously before the mixtures were allowed to phase-separate overnight. The water-rich phase (i.e., higher density mixture) was firstly drained off, and then the organic-rich phase was collected, being both phases now fully immiscible in each other. For the organic membranes (Table 1), the organic phase was used as the wetting liquid and the water phase as displacing liquid, because the alcohol-rich phase wets the polymeric structures better. On the other hand, in the case of Anopore® (aluminum oxide), the liquid roles were interchanged, with the water-rich phase used to wet the inorganic membranes to obtain better porosimetric curve results.

4. Results and Discussion

4.1.Mass loss and evaporation rate for EP technique

The PSD was characterized via EP based on the evaporation rate with time. As previous EP studies have shown [26-28, 30-32], both the mass and evaporation rate versus time plots reflect the three key phases, namely, (1) transient period, during which the temperature in the setup equilibrates; (2) free-standing liquid evaporation, during which the volatile liquid above the membrane evaporates, and thereby the mass loss with time is linear and the evaporation rate can be assumed constant despite a slight decrement; and (3) pore-liquid evaporation, during which the volatile liquid evaporates from the membrane pores. Figs. 4a and b depict respectively the representative mass and evaporation rate versus time plots, which were obtained for the Nylon membrane investigated (Table 1).

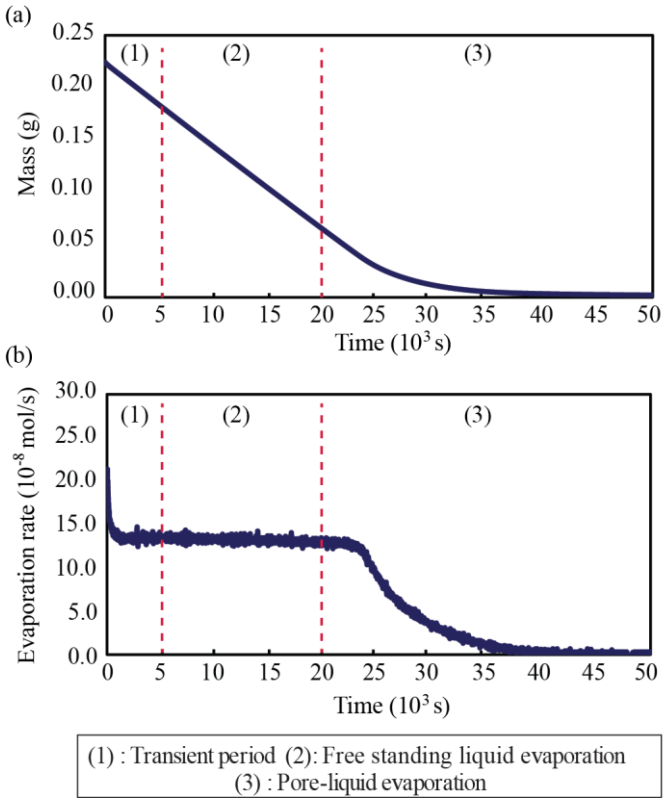

Figure 4. EP characterization: evolution of (a) net mass, and (b) evaporation rate for the Nylon membrane investigated.

4.2. Flux-pressure curve for LLDP technique

The PSD was characterized via LLDP based on the effluent (i.e., flux-pressure) curve obtained when consecutive pores of the membranes were successively subjected to flow of the displacing liquid. The resulting curve is S-shaped, as presented in Fig. 5, with the maximum slope corresponding to the moment all the pores are opened to flow so that the permeability became constant and no more pores can be opened.

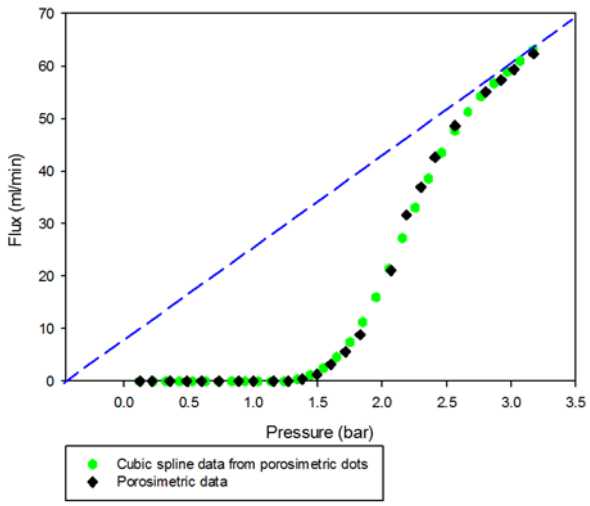

Figure 5. LLDP characterization: measured and calculated flux versus pressure plots

4.3.Comparison of pore-size distributions (PSDs)

The EP and LLDP techniques respectively provide mass-based and flow-based diameters, which in principle necessitates conversion to the same basis for a fair comparison. For the LLDP technique, the conversion of flow-based diameters to number-based ones was enabled by using the Hagen-Poiseuille model for convective transport [55]. This model assumes cylindrical geometry for the pores. Similarly, for the EP technique, the conversion from mass-based to number-based data requires the assumption of cylindrical pore geometries. Certainly this

289 geometry assumption, even being frequently used in membrane modelling, is not the case for
290 most membranes, particularly for the polymeric ones and thereby could result in compromises
291 on the resulting accuracy. Since both EP and LLDP provide the characterized diameters without
292 any assumption or calibration, this study compares the results directly despite the different
293 bases, as has been reported before [31]. In both EP and LLDP tests, three repeated runs were
294 carried out for each sample. Results from both tests, which are presented in next figures (6 to
295 11) present some sample to sample variability. This variability may be due to the own way of
296 manufacturing the membranes that result in slight differences between different areas of the
297 resulting sheet. But it also can be influenced by the fact that, in both techniques, the samples to
298 be analyzed need a previous preparation (sample wetting), which may be subject to some
299 environmental influence. In any case, the differences found are within the expected margin of
300 experimental error.

301 Figs. 6a and b display the PSDs for the Nylon membrane obtained via the EP and LLDP
302 techniques, respectively. For the EP method (Fig. 6a), the pore diameters measured in each of
303 the three runs were in the range of 5 – 130 nm, and the average pore diameter (average of the
304 mean pore diameters found for each of the three runs, d_{avg}) was 56.7 ± 3 nm. For the LLDP
305 method (Fig. 6b), the pore diameters measured were in a narrower range of 45 – 75 nm, with a
306 distinctive peak pore diameter of 59 nm, and a permeability-based d_{avg} of 57.6 ± 3 nm and
307 number-based d_{avg} of 56.3 ± 4 nm. The key observations are that: (i) the repeated PSDs were
308 similar for each technique, indicating good reproducibility and thereby reliability; (ii) the
309 permeability- and number-based d_{avg} values for LLDP were similar despite the different
310 weightings; and (iii) the d_{avg} values given by the EP and LLDP methods were in good
311 agreement, despite the different weightings and different pore diameter ranges.

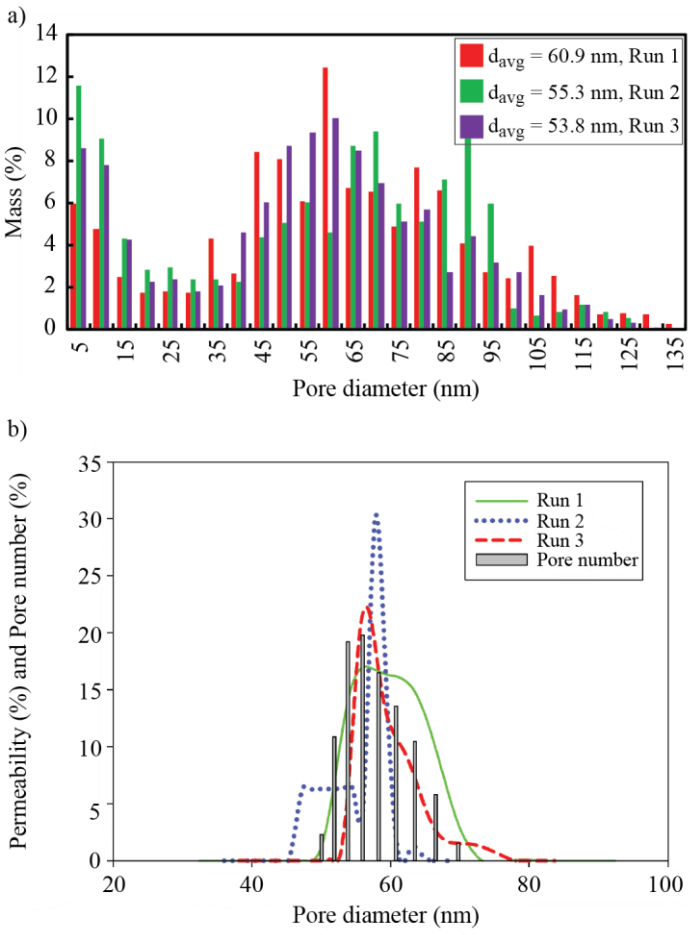

Figure 6. Pore size distributions (PSDs) of the Nylon membrane obtained using the (a) EP and (b) LLDP techniques.

The PSDs of the PES membrane are shown in Fig. 7. The d_{avg} value was 30.8 ± 2 nm by the EP technique, and the permeability- and number-based d_{avg} values were respectively 35.3 ± 9 nm and 32.9 ± 12 nm by the LLDP technique. As for the PTFE membrane (Fig. 8), the d_{avg} was 60.5 ± 4 nm by the EP technique, while 74.5 ± 2 nm for the permeability-based d_{avg} and 73.7 ± 2 nm for the number-based d_{avg} given by LLDP.

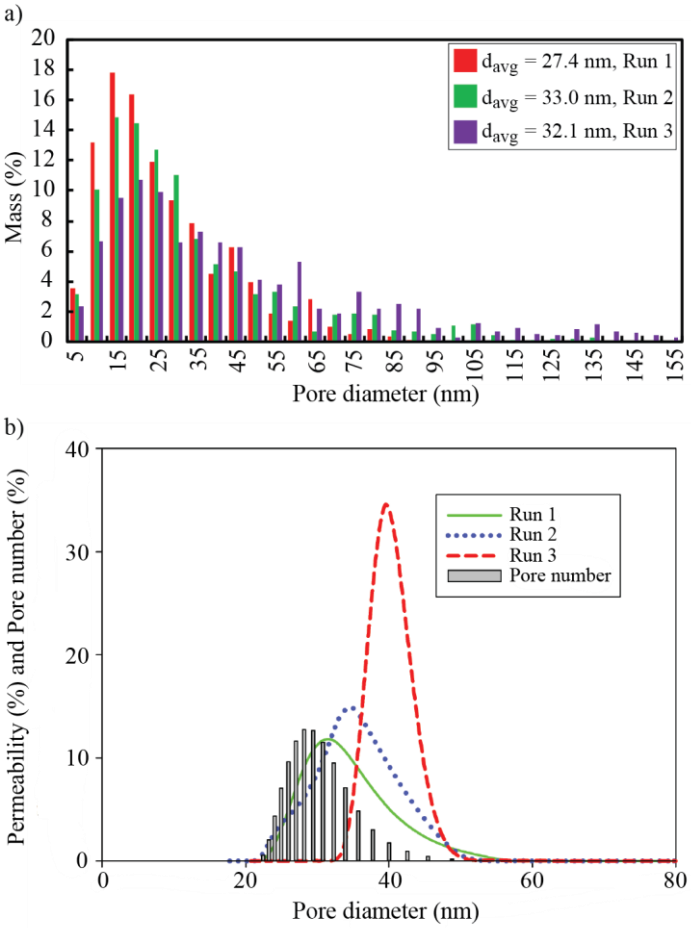

321

322 Figure 7. Pore-size distributions (PSDs) of PES membrane obtained using the (a) EP

323 and (b) LLDP techniques

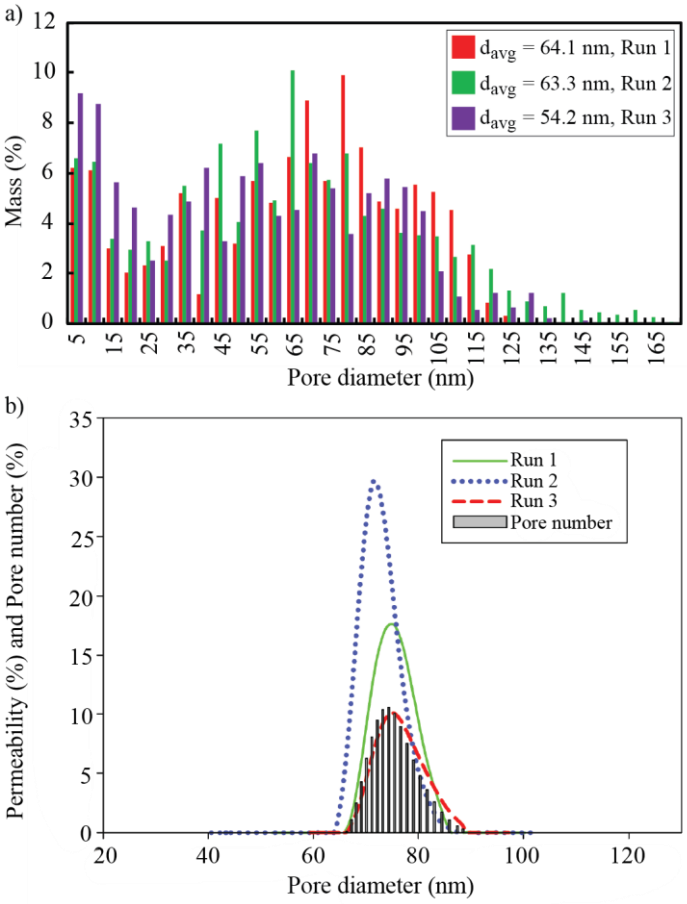

Figure 8. Pore-size distributions (PSDs) of PTFE membrane as obtained from: (a) EP and (b) LLDP techniques

Fig. 9 presents the PSDs of PET membranes. The d_{avg} was found to be 50.0 ± 5 nm via EP, and the LLDP gave the permeability-based d_{avg} as 27.2 ± 2 nm and number-based d_{avg} as 22.7 ± 9 nm. Notably, in contrast to the previous polymeric membranes, the discrepancy between EP and LLDP results is significant, with that by EP approximately twofold that by LLDP. A plausible reason is the lower mechanical strength of the PET membrane [56, 57], which caused greater compaction by the high pressures of the LLDP technique and thereby pore closure. A possible way to circumvent this is to use an alternative liquid couple with lower surface tension, which thus allows for a lower pressure during the test.

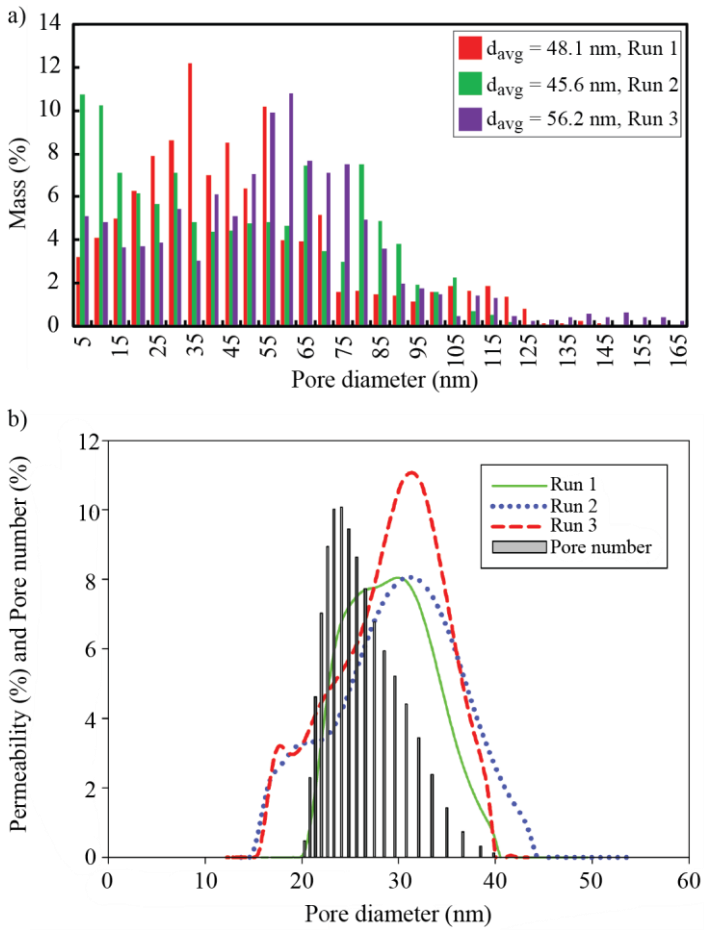

335

336 Figure 9. Pore-size distributions (PSDs) of PET membrane as obtained using the (a)

337 EP and (b) LLDP techniques

338 The PSDs of the PVDF membrane are displayed in Fig. 10. The d_{avg} values were 35.2

339 ± 0.7 nm for EP, and 61.3 ± 4 nm (permeability-based) and 51.9 ± 3 nm (number-based) for

340 LLDP measurements. The difference between the EP and LLDP results are similarly significant

341 as per that for the PET membrane. However, whereas the d_{avg} via EP was approximately twofold

342 that via LLDP for the PET membrane, it was the other way around here, specifically in that the

343 d_{avg} via EP was approximately half that via LLDP. In this case, the rubbery nature of PVDF

344 membranes caused the pores to be stretched under the high pressure during the LLDP tests and

345 thus enlarged [28].

346

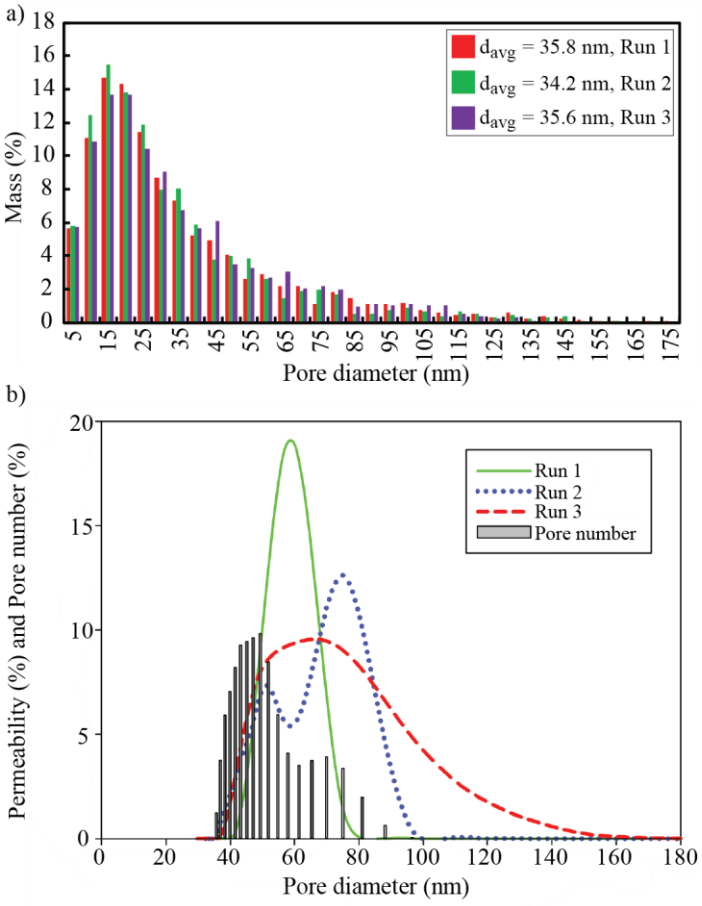

Figure 10. Pore-size distributions (PSDs) of PVDF membrane as obtained using the (a) EP and (b) LLDP techniques

The PSDs of the aluminum oxide membrane are plotted in Fig. 11. EP gave a d_{avg} of 74.7 ± 4 nm, while LLDP gave 118.3 ± 3 nm as the permeability-based d_{avg} and 115.6 ± 3 nm as the number-based d_{avg}. In view of the pores in this case being more ideal cylinders relative to the other polymeric membranes, the discrepancy in this case can be attributed to the different weightings of the d_{avg} values [58]. Specifically, since the diameter values obtained by EP has a d^2 dependency while that by LLDP has a d^4 dependency, the d_{avg} values given by LLDP is greater.

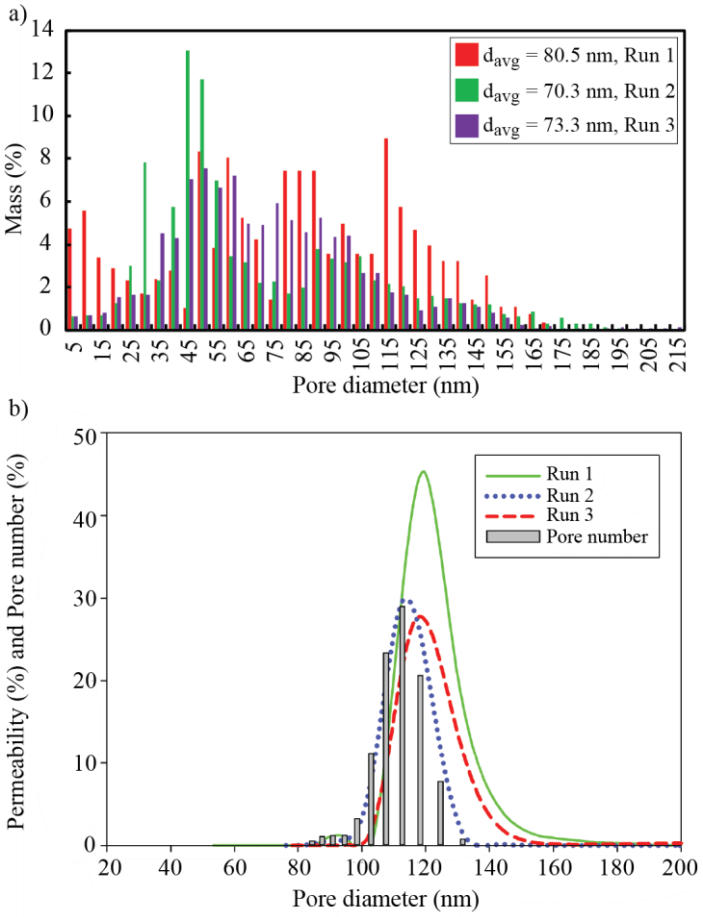

Figure 11. Pore-size distributions (PSDs) of Al_2O_3 membrane as obtained using the (a) EP and (b) LLDP techniques

4.4.Comparison of other membrane characteristics

Table 2 summarizes the d_{avg} and porosity values obtained via both EP and LLDP. As indicated earlier for d_{avg}, nylon, PES and PTFE gave better agreement of the d_{avg} values between EP and LLDP, PET and PVDF gave significant discrepancies due to the nature (e.g., mechanical strength, stretchability) of the membranes, while Al_2O_3 with more ideal pores (i.e, more cylindrical) caused some discrepancies of the d_{avg} values due to the different weightings. Also, both the d_{avg} values obtained via EP and LLDP agree reasonably well with the nominal value reported for the Al_2O_3 membrane.

With respect to porosity, Table 2 shows that the discrepancies between EP and LLDP results are much greater, with the best agreement for the Al_2O_3 membrane, and worst of an order-of-magnitude for the PVDF membrane. This is because the calculation of porosity from LLDP data relies on substitution of pore length into the Hagen-Poiseuille model, which corresponds to the membrane thickness for symmetric membranes like Al_2O_3, but only the active layer thickness for the asymmetric membranes like the polymeric ones. Because the thickness is available for the Al_2O_3 membrane through measurement with a pair of Vernier calipers and the PES membrane through SEM (scanning electronic microscope) images of the cross-section, these porosity values via LLDP of these two membranes agree best with that of EP. For the rest of the membranes, a reasonable value of 10 μm was used as an estimation of active layer thickness. Unfortunately, most UF membranes are asymmetric, which necessitates cross-sectional SEM images to determine the active layer that is typically not distinctly demarcated from the porous support.

Table 2: Mean pore diameters (d_{avg}) and porosity values obtained via EP and LLDP for the six membranes investigated. Errors are calculated as percentage of the corresponding value.

		EP		LLDP		
Membrane	**Nominal d_{avg} (nm)**	d_{avg} **(nm)**	**Porosity %**	d_{avg} **(nm) (Number-based)**	d_{avg} **(nm) (Permeability-based)**	**Porosity %**
Nylon	Not available	56.7±5	56.9±15	56.3±4	57.6±3	11.3±0.5
PES	Not available	30.8±8	69.8±5	32.9±12	35.3±9	34±4
PTFE	Not available	60.5±7	80.7±3	73.7±2	74.5±2	13.0±0.5
PET	Not available	50±9	78.9±2	22.7±9	27.2±2	15.8±1.2
PVDF	Not available	35.2±3	87.2±3	51.9±3	61.3±4	1.7±0. 4
Al_2O_3	100	75.7±6	71.7±5	115.6±3	118.3 ±3	61±15

Table 3 compares the reported and measured (via LLDP) MWCO (molecular weight cut-off) values, since UF membranes are typically selected based on the MWCO value supplied by the manufacturer. Unfortunately, EP currently does not explicitly give MWCO, though it has been reported in an earlier study that the MWCO is equivalent to the 90th percentile (number-

390 based) pore diameter [31]. Out of the five MWCO values measured by LLDP, only that for PES
391 and PET were in the typical UF range. Also, for PES and PVDF membranes that the MWCO
392 values are available for, the LLDP gave values greater than the nominal ones, with that for
393 PVDF being more than 10 times that of the nominal value. It should be noted that MWCO refers
394 to the 90% retention value, which thereby is governed by the largest pores in the distribution.
395 Even if the mean pore diameters (Table 2) gave reasonable values, errors associated with the
396 measurement of the first (largest) pores at the lowest pressures would cause the cut-off values
397 to be overestimated. This can be circumvented by the use of another liquid pair with higher
398 surface tension and thereby greater accuracy in the equilibrium pressure determination. It also
399 must be noted that all empirical correlations used to estimate molecular weight from molecule
400 size are based on power laws that magnify small errors in the pore size calculations [45].

401
402 Table 3: Comparison of nominal and measured MWCO values

Membrane	Nominal MWCO (kDa)	LLDP MWCO (kDa)
Nylon	Not available	1460
PES	300	470
PTFE	Not available	2570
PET	Not available	350
PVDF	100	1150

403

404 **5. Conclusions**

405 This study compared the pore size distribution measurements obtained by using the
406 Evapoporometry (EP) and Liquid-Liquid Displacement Porosity (LLDP) techniques for the
407 analysis of six UF/MF membranes, namely, five polymeric ones (i.e., nylon, PES, PTFE, PET,
408 and PVDF) and one inorganic (i.e., alumina). Both methods have been used in the past for the
409 characterization of commercial membranes; thus, the comparative assessment presented here
410 was aimed at a better understanding of the differences, capabilities, and potential of these
411 relatively new membrane characterization methods. It should be noted that LLDP characterizes

412 the pore throat (i.e., narrowest cross-sectional diameter of the pore), while EP the pore diameter
413 at the evaporating liquid surface. Therefore EP accounts for both continuous and dead-ended
414 pores while LLDP only measures flow-through pores. Accordingly, some slight differences
415 between both techniques are reasonably expected.

416 Three key results regarding d_{avg} are described as follows. Firstly, for three of the polymeric
417 membranes, namely, nylon, PES and PTFE, the d_{avg} values given by the EP and LLDP methods
418 were in good agreement, despite the different weightings and different pore diameter ranges.
419 Both EP and LLDP techniques provide directly information regarding, respectively mass-based
420 and flow-based diameters. While, the conversion to number-based distributions for LLDP
421 (applying Hagen-Poiseuille model) and for EP requires assumption of a cylindrical pore
422 geometry which compromises the resulting accuracy, as it not normally fulfilled. Therefore, the
423 measured diameters, that are without any assumption or calibration, are used directly for
424 comparison. Secondly, the d_{avg} value given by EP was approximately twice that by LLDP for
425 PET, whereas half that by LLDP for PVDF. This can be linked to the higher pressure during
426 LLDP testing. Specifically, the high pressure caused the lower mechanical strength PET to be
427 subject to pore closure upon compaction that resulted in lower d_{avg} values, while the rubbery
428 PVDF was subject to pore-stretching that led to higher d_{avg} values. This highlights the adverse
429 effect of pressure on the membranes, but can be circumvented by choosing a different liquid
430 pair that would require a lower pressure. Thirdly, for the inorganic alumina membrane, the d_{avg}
431 values determined by both EP and LLDP agree reasonably well with that provided by the
432 manufacturer. Due to the more ideal cylindrical pores of this membrane, the d^4-weighting of
433 the LLDP measurement gave a greater d_{avg} value than that of the d^2-weighting of the EP
434 measurement.

435 Regarding porosity, reasonable agreements between EP and LLDP were only obtained for
436 the PES and alumina membranes, for which the thicknesses of the active layers were explicitly

known. While EP does not require the active layer thickness as an input, this parameter is needed in the Hagen-Poiseuille model used for LLDP. With respect to MWCO, the LLDP generally over-estimated the values, because of the errors associated with the measurement of the first (largest) pores at the lowest pressures. This can be circumvented by the use of another liquid pair with higher surface tension and thereby greater accuracy in the equilibrium pressure determination.

Table 4: Advantages and disadvantages of EP and LLDP to determine PSD of membranes

Method	Advantages	Disadvantages
EP	- Mass-based PSD† at sample surface - large sample size - high accuracy of gravimetric measurement - measurement at ambient conditions - it uses readily available and inexpensive laboratory equipment - it can characterize biofouling layer	- Indirect method based on Kelvin equation - decreasing accuracy with increasing pore diameter - includes information about dead-ended pores - adsorbed t-layer correction required
LLDP	- Flow-based PSD† - it can test both large or small sample size - determines smallest diameter in pores open to flow - adaptable for different membrane configurations (flat, tubular, fibbers) - it can be used to estimate cut-off	- Indirect method based on Young-Laplace equation - flow-based measurement less sensitive to small pores - requires high pressure for very small pores - cannot characterize biofouling layer - pairs of liquids with lower surface tension would improve applicability
Common	- minimal sample preparation, small footprint and simple procedure - pore geometry not assumed for direct results - they characterize UF and MF membranes - fast, reliable and accurate analysis - they can determine the effect of fouling	- Pore geometry assumption needed to convert data into a different calculation basis - extension to NF requires stretching limits of their theoretical basis - less accurate when dealing with low porosity membranes - interconnecting pores could affect results - sensible to sample wettability

Some advantages and disadvantages (some of them common to both) from studied techniques are shown in Table 4, arising from this study and previous experience of both research labs. To summarize, both EP and LLDP techniques are suitable characterizing the PSD and mean pore diameters for UF/tight MF membranes, giving important information that could be related to membrane performance and retention capabilities. Surely, a better understanding of the underlying reason of such observed differences particularly for the PET, PVDF and Al_2O_3 membranes is needed, which could result from the application of different liquids with different surface tension values and better wettability.

Acknowledgment

We acknowledge funding from the Merlion Singapore-France Grant and the GSK (GlaxoSmithKline) – EDB (Economic Development Board) Trust Fund (Singapore). Also, we would like to acknowledge the support of the European Regional Development Fund (in the framework of the Interreg Sudoe programme) for funding the Project "PEMFC - SUDOE" - SOE1/P1/E0293.

Nomenclature

ΔL_k	Differential permeability in step k; (k=1...i) ($m^3/s/Pa$)
ΔP	Hydraulic pressure (Pa)
ΔP_k	Applied pressure corresponding to the kth of analysis; (k=1...i) (Pa)
d_k	Pore diameter of the pores opened in step k (k= 1,. . .,i) (m)
d	Equivalent pore diameter (m)
H	Mean curvature (m^{-1})
L_k	Hydraulic permeability in step k ; (k=1...i) ($m^3/s/Pa$)
L_{tot}	Total Hydraulic permeability in step k=i ; (Asymptotic permeability) ($m^3/s/Pa$)
l	Pore length (m)
n_k	Number of pores opened in step k; (k= 1,. . ., i) (dimensionless)
P_0	Total Pressure (Pa)
$P_{L,V}$	Liquid/Vapor phase pressure (Pa)
P^0_A	Normal vapor pressure of the volatile wetting liquid (Pa)
P_A	Vapor pressure of the volatile wetting liquid (Pa)
Q_k	Volumetric flow corresponding to the kth step of analysis (m^3/s)
r	Equivalent pore radius (m)
R	Gas constant=8.3145 (J/mol·K)
T	Temperature (K)
$V_{L,V}$	Liquid/Vapor molar volume (m^3/mol)
W^0_A	Evaporation rate of liquid A during pore draining (mol/s)
W_A	Evaporation rate of liquid A overlying the membrane (mol/s)

488 ***Greek letters***

489	η	Dynamic viscosity of the displacing liquid (Pa s)
490	γ	Interfacial tension of the liquid/vapor pairs (mN/m)
491	θ	Contact angle (°)
492	μ_L	Chemical potential of the liquid phase (J/mol)
493	μ_V	Chemical potential of the vapor phase (J/mol)

494

495 ## References

496 [1] G. Owen, M. Bandi, J.A. Howell, S.J. Churchouse, Economic assessment of membrane processes for
497 water and waste water treatment, Journal of Membrane Science, 102 (1995) 77-91.
498 [2] Z.F. Cui, Y. Jiang, R.W. Field, Chapter 1 - Fundamentals of Pressure-Driven Membrane Separation
499 Processes, in: Z.F. Cui, H.S. Muralidhara (Eds.) Membrane Technology, Butterworth-Heinemann,
500 Oxford, 2010, pp. 1-18.
501 [3] J.I. Calvo, A. Bottino, G. Capannelli, A. Hernández, Comparison of liquid–liquid displacement
502 porosimetry and scanning electron microscopy image analysis to characterise ultrafiltration track-
503 etched membranes, Journal of Membrane Science, 239 (2004) 189-197.
504 [4] N.A. Ochoa, P. Prádanos, L. Palacio, C. Pagliero, J. Marchese, A. Hernández, Pore size distributions
505 based on AFM imaging and retention of multidisperse polymer solutes: Characterisation of
506 polyethersulfone UF membranes with dopes containing different PVP, Journal of Membrane Science,
507 187 (2001) 227-237.
508 [5] H. Reingruber, A. Zankel, C. Mayrhofer, P. Poelt, A new in situ method for the characterization of
509 membranes in a wet state in the environmental scanning electron microscope, Journal of Membrane
510 Science, 399-400 (2012) 86-94.
511 [6] M. Baklanov, K. P. Mogilnikov, V. Polovinkin, F. Dultsev, Determination of pore size distribution in
512 thin films by ellipsometric porosimetry, 2000.
513 [7] T.C. Chilcott, M. Chan, L. Gaedt, T. Nantawisarakul, A.G. Fane, H.G.L. Coster, Electrical impedance
514 spectroscopy characterisation of conducting membranes: I. Theory, Journal of Membrane Science, 195
515 (2002) 153-167.
516 [8] H. D. Bale, Small-Angle X-Ray-Scattering Investigation of Submicroscopic Porosity with Fractal
517 Properties, 1984.
518 [9] K. Darowicki, M. Szociński, Local impedance spectroscopy of membranes, Journal of Membrane
519 Science, 303 (2007) 1-3.
520 [10] J.-D. Jeon, S.J. Kim, S.-Y. Kwak, 1H nuclear magnetic resonance (NMR) cryoporometry as a tool to
521 determine the pore size distribution of ultrafiltration membranes, Journal of Membrane Science, 309
522 (2008) 233-238.
523 [11] K.C. Khulbe, B. Kruczek, G. Chowdhury, S. Gagné, T. Matsuura, S.P. Verma, Characterization of
524 membranes prepared from PPO by Raman scattering and atomic force microscopy, Journal of
525 Membrane Science, 111 (1996) 57-70.
526 [12] K.C. Khulbe, T. Matsuura, Characterization of synthetic membranes by Raman spectroscopy,
527 electron spin resonance, and atomic force microscopy; a review, Polymer, 41 (2000) 1917-1935.
528 [13] K.C. Khulbe, T. Matsuura, C.Y. Feng, Study on cellulose acetate membranes for reverse osmosis
529 and polyethersulfone membranes for ultrafiltration by electron spin resonance technique,
530 Desalination, 148 (2002) 329-332.

[14] K.C. Khulbe, T. Matsuura, G. Lamarche, A.M. Lamarche, C. Choi, S.H. Noh, Study of the structure of asymmetric cellulose acetate membranes for reverse osmosis using electron spin resonance (ESR) method, Polymer, 42 (2001) 6479-6484.
[15] R. Lamsal, S.G. Harroun, C.L. Brosseau, G.A. Gagnon, Use of surface enhanced Raman spectroscopy for studying fouling on nanofiltration membrane, Separation and Purification Technology, 96 (2012) 7-11.
[16] D. Nanda, K.-L. Tung, W.-S. Hung, C.-H. Lo, Y.-C. Jean, K.-R. Lee, C.-C. Hu, J.-Y. Lai, Characterization of fouled nanofiltration membranes using positron annihilation spectroscopy, Journal of Membrane Science, 382 (2011) 124-134.
[17] P.S. Singh, P. Ray, Z. Xie, M. Hoang, Synchrotron SAXS to probe cross-linked network of polyamide 'reverse osmosis' and 'nanofiltration' membranes, Journal of Membrane Science, 421-422 (2012) 51-59.
[18] H.-K. Song, Y.-H. Jung, K.-H. Lee, L.H. Dao, Electrochemical impedance spectroscopy of porous electrodes: the effect of pore size distribution, Electrochimica Acta, 44 (1999) 3513-3519.
[19] K.-L. Tung, Y.-C. Jean, D. Nanda, K.-R. Lee, W.-S. Hung, C.-H. Lo, J.-Y. Lai, Characterization of multilayer nanofiltration membranes using positron annihilation spectroscopy, Journal of Membrane Science, 343 (2009) 147-156.
[20] E.P. Barrett, L.G. Joyner, P.P. Halenda, The Determination of Pore Volume and Area Distributions in Porous Substances. I. Computations from Nitrogen Isotherms, Journal of the American Chemical Society, 73 (1951) 373-380.
[21] C. Pierce, Computation of Pore Size from Physical Adsorption Data, 1953.
[22] F.P. Cuperus, D. Bargeman, C.A. Smolders, PERMPOROMETRY - THE DETERMINATION OF THE SIZE DISTRIBUTION OF ACTIVE PORES IN UF MEMBRANES, Journal of Membrane Science, 71 (1992) 57-67.
[23] C. Eyraud, M. Betemps, J.F. Quinson, F. Chatelut, M. Brun, B. Rasneur, DETERMINATION OF THE PORE-SIZE DISTRIBUTION OF AN ULTRAFILTER BY - GAS-LIQUID PERMPOROMETRY MEASUREMENT - COMPARISON BETWEEN FLOW POROMETRY AND CONDENSATE EQUILIBRIUM POROMETRY, Bulletin De La Societe Chimique De France Partie I-Physicochimie Des Systemes Liquides Electrochimie Catalyse Genie Chimique, (1984) I237-I244.
[24] M.G. Katz, G. Baruch, New insights into the structure of microporous membranes obtained using a new pore size evaluation method, Desalination, 58 (1986) 199-211.
[25] A. Mey-Marom, M.G. Katz, Measurement of active pore size distribution of microporous membranes - a new approach, Journal of Membrane Science, 27 (1986) 119-130.
[26] E. Akhondi, F. Wicaksana, W.B. Krantz, A.G. Fane, Evapoporometry determination of pore-size distribution and pore fouling of hollow fiber membranes, Journal of Membrane Science, 470 (2014) 334-345.
[27] E. Akhondi, F. Zamani, J.W. Chew, W.B. Krantz, A.G. Fane, Improved design and protocol for evapoporometry determination of the pore-size distribution, Journal of Membrane Science, 496 (2015) 334-343.
[28] E. Akhondi, F. Zamani, A.W.K. Law, W.B. Krantz, A.G. Fane, J.W. Chew, Influence of backwashing on the pore size of hollow fiber ultrafiltration membranes, Journal of Membrane Science, 521 (2017) 33-42.
[29] S. Goh, Q. Zhang, J. Zhang, D. McDougald, W.B. Krantz, Y. Liu, A.G. Fane, Impact of a biofouling layer on the vapor pressure driving force and performance of a membrane distillation process, Journal of Membrane Science, 438 (2013) 140-152.
[30] W.B. Krantz, A.R. Greenberg, E. Kujundzic, A. Yeo, S.S. Hosseini, Evapoporometry: A novel technique for determining the pore-size distribution of membranes, Journal of Membrane Science, 438 (2013) 153-166.
[31] F. Zamani, E. Akhondi, G.H. Koops, W.B. Krantz, A.G. Fane, J.W. Chew, Evapoporometry adaptation to determine the lumen-side pore-size distribution (PSD) of hollow fiber and tubular membranes, Journal of Membrane Science, 526 (2017) 1-8.
[32] F. Zamani, P. Jayaraman, E. Akhondi, W.B. Krantz, A.G. Fane, J.W. Chew, Extending the uppermost pore diameter measureable via Evapoporometry, Journal of Membrane Science, 524 (2017) 637-643.

583 [33] M.B. Tanis-Kanbur, F. Zamani, W.B. Krantz, X. Hu, J.W. Chew, Adaptation of Evapoporometry (EP)
584 to Characterize the Continuous Pores and Interpore Connectivity in Polymeric Membranes, Journal of
585 Membrane Science, (2018).
586 [34] M. Brun, A. Lallemand, J.-F. Quinson, C. Eyraud, A new method for the simultaneous determination
587 of the size and shape of pores: the thermoporometry, Thermochimica Acta, 21 (1977) 59-88.
588 [35] K. Kaneko, DETERMINATION OF PORE-SIZE AND PORE-SIZE DISTRIBUTION .1. ADSORBENTS AND
589 CATALYSTS, Journal of Membrane Science, 96 (1994) 59-89.
590 [36] N. Kononenko, V. Nikonenko, D. Grande, C. Larchet, L. Dammak, M. Fomenko, Y. Volfkovich,
591 Porous structure of ion exchange membranes investigated by various techniques, Advances in Colloid
592 and Interface Science, 246 (2017) 196-216.
593 [37] P.A. Monson, Understanding adsorption/desorption hysteresis for fluids in mesoporous materials
594 using simple molecular models and classical density functional theory, Microporous and Mesoporous
595 Materials, 160 (2012) 47-66.
596 [38] A. Bottino, G. Capannelli, A. Grosso, O. Monticelli, M. Nicchia, Porosimetric Characterization of
597 Inorganic Membranes, Separation Science and Technology, 29 (1994) 985-999.
598 [39] A. Bottino, G. Capannelli, P. Petit-bon, N. Cao, M. Pegoraro, G. Zoia, Pore Size and Pore-Size
599 Distribution in Microfiltration Membranes, Separation Science and Technology, 26 (1991) 1315-1327.
600 [40] A. Jena, K. Gupta, Advances in Pore Structure Evaluation by Porometry, Chemical Engineering &
601 Technology, 33 (2010) 1241-1250.
602 [41] M.C. Almécija, J.E. Zapata, A. Martinez-Ferez, A. Guadix, A. Hernández, J.I. Calvo, E.M. Guadix,
603 Analysis of cleaning protocols in ceramic membranes by liquid–liquid displacement porosimetry,
604 Desalination, 245 (2009) 541-545.
605 [42] E. Antón, J.I. Calvo, J.R. Álvarez, A. Hernández, S. Luque, Fitting approach to liquid–liquid
606 displacement porosimetry based on the log-normal pore size distribution, Journal of Membrane
607 Science, 470 (2014) 219-228.
608 [43] J.I. Calvo, A. Bottino, G. Capannelli, A. Hernández, Pore size distribution of ceramic UF membranes
609 by liquid–liquid displacement porosimetry, Journal of Membrane Science, 310 (2008) 531-538.
610 [44] J.I. Calvo, R.I. Peinador, P. Prádanos, A. Bottino, A. Comite, R. Firpo, A. Hernández, Porosimetric
611 characterization of polysulfone ultrafiltration membranes by image analysis and liquid–liquid
612 displacement technique, Desalination, 357 (2015) 84-92.
613 [45] J.I. Calvo, R.I. Peinador, P. Prádanos, L. Palacio, A. Bottino, G. Capannelli, A. Hernández, Liquid–
614 liquid displacement porometry to estimate the molecular weight cut-off of ultrafiltration membranes,
615 Desalination, 268 (2011) 174-181.
616 [46] J.I. Calvo, R.I. Peinador, V. Thom, T. Schleuss, K. ToVinh, P. Prádanos, A. Hernández, Comparison
617 of pore size distributions from dextran retention tests and liquid-liquid displacement porosimetry,
618 Microporous and Mesoporous Materials, 250 (2017) 170-176.
619 [47] P. Carretero, S. Molina, A. Lozano, J. de Abajo, J.I. Calvo, P. Prádanos, L. Palacio, A. Hernández,
620 Liquid–liquid displacement porosimetry applied to several MF and UF membranes, Desalination, 327
621 (2013) 14-23.
622 [48] R.I. Peinador, J.I. Calvo, P. Prádanos, L. Palacio, A. Hernández, Characterisation of polymeric UF
623 membranes by liquid–liquid displacement porosimetry, Journal of Membrane Science, 348 (2010) 238-
624 244.
625 [49] R.I. Peinador, J.I. Calvo, K. ToVinh, V. Thom, P. Prádanos, A. Hernández, Liquid–liquid displacement
626 porosimetry for the characterization of virus retentive membranes, Journal of Membrane Science, 372
627 (2011) 366-372.
628 [50] L. Zheng, H. Li, H. Yu, G. Kang, T. Xu, J. Yu, X. Li, H. Xu, “Modified” Liquid–Liquid Displacement
629 Porometry and Its Applications in Pd-Based Composite Membranes, Membranes, 8 (2018).
630 [51] L.R. Fisher, J.N. Israelachvili, Experimental studies on the applicability of the Kelvin equation to
631 highly curved concave menisci, Journal of Colloid and Interface Science, 80 (1981) 528-541.
632 [52] A.C. Mitropoulos, The Kelvin equation, Journal of Colloid and Interface Science, 317 (2008) 643-
633 648.

[53] T. Takei, M. Chikazawa, T. Kanazawa, Validity of the Kelvin equation in estimation of small pore size by nitrogen adsorption, Colloid and Polymer Science, 275 (1997) 1156-1161.
[54] T. Courtois, Dispositif de mesure de caractéristiques liées a la porosité des media poreux, in: F. Patent (Ed.), France, 2003.
[55] S.N. P. Grabar, Sur le diamètre des pores des membranes en collodion utilisées en ultrafiltration, J. Chim. Phys, 33 721–741.
[56] K. Wang, A.A. Abdala, N. Hilal, M.K. Khraisheh, Chapter 13 - Mechanical Characterization of Membranes, in: N. Hilal, A.F. Ismail, T. Matsuura, D. Oatley-Radcliffe (Eds.) Membrane Characterization, Elsevier, 2017, pp. 259-306.
[57] F. Kayaci, Z. Aytac, T. Uyar, Surface modification of electrospun polyester nanofibers with cyclodextrin polymer for the removal of phenanthrene from aqueous solution, Journal of Hazardous Materials, 261 (2013) 286-294.
[58] M.J. Rhodes, Chapter 1, Introduction to particle technology, in, John Wiley, Chichester ; New York, 1998, pp. xiii, 320 p.